Micromechanical Circuits for Communication Transceivers

C. T.-C. Nguyen, "Micromechanical circuits for communication transceivers (invited)," *Proceedings*, 2000 Bipolar/BiCMOS Circuits and Technology Meeting (BCTM), Minneapolis, Minnesota, September 25-26, 2000, pp. 142-149.

Clark T.-C. Nguyen

Center for Integrated Microsystems
Department of Electrical Engineering and Computer Science
University of Michigan
Ann Arbor, Michigan 48109-2122

ABSTRACT: Micromechanical (or "μmechanical) communication circuits fabricated via IC-compatible MEMS technologies and capable of low-loss filtering, mixing, switching, and frequency generation, are described with the intent to miniaturize wireless transceivers. Receiver architectures are then proposed that best harness the tiny size, zero dc power dissipation, and ultra-high-*Q* of vibrating μmechanical resonator circuits. Among the more aggressive architectures proposed are one based on a μmechanical RF channel-selector and one featuring an all-MEMS RF front-end. These architectures maximize performance gains by using highly selective, low-loss μmechanical circuits on a massive scale, taking full advantage of *Q* versus power trade-offs. Micromechanical filters, mixer-filters, and switchable synthesizers are identified as key blocks capable of substantial power savings when used in the aforementioned architectures. As a result of this architectural exercise, more focused directions for further research and development in RF MEMS are identified.

I. Introduction

Due to their need for high frequency selectivity and low noise frequency manipulation, portable wireless communication transceivers continue to rely on off-chip resonator technologies that interface with transistor electronics at the board-level. In particular, highly selective, low loss radio frequency (RF) and intermediate frequency (IF) bandpass filters generally require ceramic, SAW, or quartz acoustic resonator technologies, with *Q*'s in excess of 1,000. In addition, *LC* resonator tanks with *Q*'s greater than 30 are required by voltage-controlled oscillators (VCO's) to achieve sufficiently low phase noise. These off-chip resonator components then contribute to the substantial percentage (often up to 80%) of portable transceiver area taken up by board-level, passive components.

Recent advances in IC-compatible microelectromechanical system (MEMS) technologies that make possible micro-scale, mechanical circuits capable of low-loss filtering, mixing, switching, and frequency generation, now suggest methods for board-less integration of wireless transceiver components [1]. In fact, given the existence already of technologies that merge micromechanics with transistor circuits onto single silicon chips [2-5], single-chip transceivers may eventually be possible, perhaps using alternative architectures that maximize the use of passive, high-*Q*, μmechanical circuits to reduce power consumption for portable applications. This paper presents an overview of the μmechanical circuits and associated technologies expected to play key roles in reducing the size and power consumption of future communication transceivers.

II. Micromechanical Circuits

Although mechanical circuits, such as quartz crystal resonators and SAW filters, provide essential functions in the majority of transceiver designs, their numbers are generally suppressed due to their large size and finite cost. Unfortunately, when minimizing the use of high-*Q* components, designers often trade power for selectivity (i.e., *Q*), and hence, sacrifice transceiver performance. As a simple illustration, if the high-*Q* IF filter in the receive path of a communication sub-system is removed, the dynamic range requirement on the subsequent IF amplifier, IQ mixer, and A/D converter circuits, increases dramatically, forcing a corresponding increase in power consumption. Similar trade-offs exist at RF, where the larger the number or greater the complexity of high-*Q* components used, the smaller the power consumption in surrounding transistor circuits.

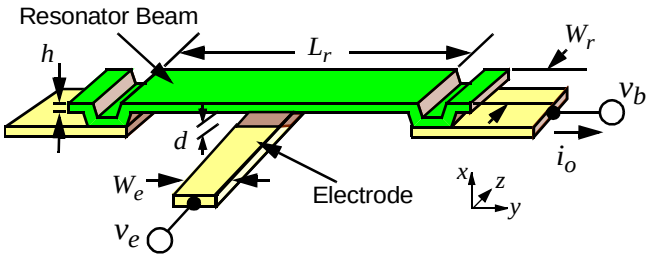

Fig. 1: Schematic of a clamped-clamped beam μmechanical resonator in a general bias and excitation configuration.

By shrinking dimensions and introducing batch fabrication techniques, MEMS technology provides a means for relaxing the present constraints on the number and complexity of mechanical circuits, perhaps with implications not unlike those that integrated circuit technology had on transistor circuit complexity. In particular, since they can now be integrated (perhaps on a massive scale) using MEMS technology, vibrating μmechanical resonators (or μmechanical links) can now be thought of as tiny circuit elements, much like resistors or transistors, in a new mechanical circuit technology. Like a single transistor, a single mechanical link does not possess adequate processing power for most applications. However, again like transistors, when combined into larger (potentially, VLSI) circuits, the true power of μmechanical links can be unleashed, and signal processing functions with attributes previously inaccessible to transistor circuits may become feasible. This in turn can lead to architectural changes for communication transceivers. MEMS technology may in fact make its most important impact not at the component level, but at the system level, by offering alternative transceiver architectures that emphasize selectivity to substantially reduce power consumption and enhance performance [6].

Before exploring the architectural implications, specific μmechanical circuits are first reviewed, starting with the basic building block elements used for mechanical circuits, then expanding with descriptions of the some of most useful linear and nonlinear mechanical circuits.

A. The Micromechanical Beam Element

To date, the majority of μmechanical circuits most useful for communication functions have been realized using μmechanical flexural-mode beam elements, such as presented in Fig. 1 with clamped-clamped boundary conditions. As shown, this device consists of a beam anchored (i.e., clamped) at both ends, with an electrode underlying its central locations. Both the beam and electrode are constructed of conductive materials, such as metal, or doped silicon. Although several micromachining technologies are available to realize such an element in a variety of different materials, surface micromachining has been the preferred method for μmechanical communication circuits, mainly due to its flexibility

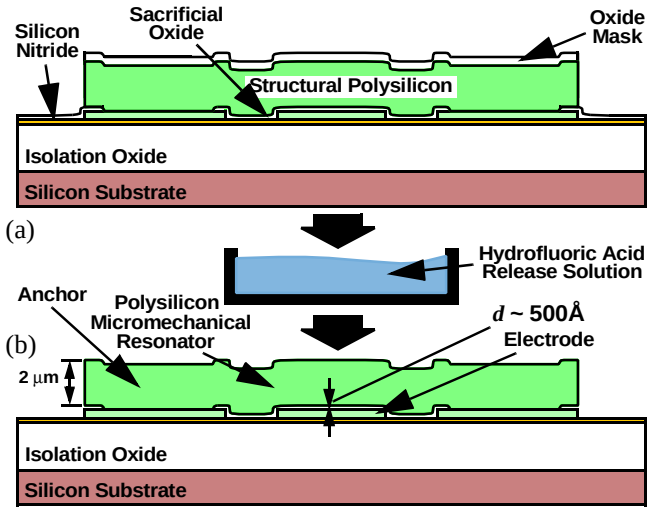

Fig. 2: Cross-sections describing surface micromachining. (a) Required film layers up to the release etch step. (b) Resulting free-standing beam following a release etch in HF [8].

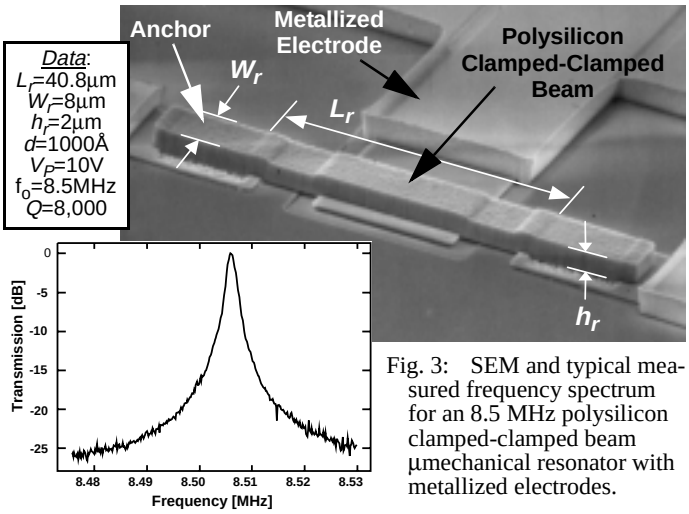

Fig. 3: SEM and typical measured frequency spectrum for an 8.5 MHz polysilicon clamped-clamped beam μmechanical resonator with metallized electrodes.

in providing a variety of beam end conditions and electrode locations, and its ability to realize very complex geometries with multiple levels of suspension.

Figure 2 summarizes the essential elements of a typical surface-micromachining process [7] tailored to produce a clamped-clamped beam [8]. In this process, a series of film depositions and lithographic patterning steps—identical to similar steps used in planar IC fabrication technologies—are utilized to first achieve the cross-section shown in Fig. 2(a). Here, a sacrificial oxide layer supports the structural polysilicon material during deposition, patterning, and subsequent annealing. In the final step of the process, the wafer containing cross-sections similar to Fig. 2(a) is dipped into a solution of hydrofluoric acid, which etches away the sacrificial oxide layer without significantly attacking the polysilicon structural material. This leaves the free-standing structure shown in Fig. 2(b), capable of movement in multiple dimensions, if necessary, and more importantly, capable of vibrating with high Q and good temperature stability, with temperature coefficients on the order of −10 ppm/°C [9]. Figure 3 presents the scanning electron micrograph (SEM) and typical measured frequency spectrum for a clamped-clamped beam polysilicon μmechanical resonator designed to operate at 8.5 MHz with a Q of 8,000.

Returning to Fig. 1, the μmechanical beam element normally accepts two electrical inputs, v_e and v_b, applied to the electrode and beam, respectively. In this configuration, the difference voltage $(v_e - v_b)$ is effectively applied across the electrode-to-resonator capacitor gap, generating a force between the stationary electrode and movable beam given by

$$F_d = \frac{\partial E}{\partial x} = \frac{1}{2}(v_e - v_b)^2 \frac{\partial C}{\partial x} = \frac{1}{2}(v_b^2 - 2v_b v_e + v_e^2)\frac{\partial C}{\partial x} \qquad (1)$$

where x is displacement (with direction indicated in Fig. 1), and $(\partial C/\partial x)$ is the change in resonator-to-electrode capacitance per unit displacement (and is negative with the directions indicated in Fig. 1). Depending upon the type and frequency of the voltages applied to terminals e and b, this force can be tailored to specify any one of a variety of signal processing functions available to the beam element. These functions are now described.

B. Micromechanical Reference Tanks

The high Q and thermal stability of the resonance frequency of single μmechanical beam elements make them good candidates for use as tanks in reference oscillator applications. When used as a tank or filter circuit (as opposed to a mixer or switch, to be discussed later), a dc-bias voltage V_P is applied to the conductive beam, while an ac excitation signal $v_i = V_i \cos\omega_i t$ is applied to the underlying electrode. In this configuration, (1) reduces to

$$F_d = \frac{\partial C}{\partial x}\left(\frac{V_P^2}{2} + \frac{V_i^2}{4}\right) - V_P \frac{\partial C}{\partial x} V_i \cos\omega_i t + \frac{\partial C}{\partial x}\frac{V_i}{4}\cos 2\omega_i t \qquad (2)$$

The first term in (2) represents an off-resonance dc force that statically bends the beam, but that otherwise has little effect on its frequency processing function, especially for VHF and above frequencies. The second term constitutes a force at the frequency of the input signal, amplified by the dc-bias voltage V_P, and is the main input component used in tank and filter applications. When $\omega_i = \omega_o$ (the radian resonance frequency) this force drives the beam into resonance, creating a dc-biased (via V_P) time-varying capacitance between the electrode and resonator, and sourcing an output current $i_o = -V_P(\partial C/\partial x)(\partial x/\partial t)$. When plotted versus the frequency of v_i, i_o traces out a bandpass biquad characteristic with a Q ~10,000 (c.f., Fig. 4)—very suitable for reference oscillators.

The third term in (2) represents a term capable of driving the beam into vibration when $\omega_i = (1/2)\omega_o$. If V_P is very large compared with V_i, this term is greatly suppressed, but can be troublesome for bandpass filters in cases where very large interferers are present at half the passband frequency. In these cases, a μmechanical notch filter at $(1/2)\omega_o$ may be needed.

The vibrational resonance frequency of the clamped-clamped beam of Fig. 1 is given by the expression [8,10]

$$f_o = \frac{1}{2\pi}\sqrt{\frac{k_r}{m_r}} = 1.03\kappa\sqrt{\frac{E}{\rho}}\frac{h}{L_r^2}(1 - g(V_P))^{1/2}, \qquad (3)$$

where E and ρ are the Young's modulus and density of the structural material, respectively; h and L_r are specified in Fig. 1; κ is a scaling factor that models the effects of surface topography in actual implementations; and g is a function modeling a V_P-dependent electrical stiffness. From (3), geometry clearly plays a major role in setting the resonance frequency, and in practice, attaining a specified frequency amounts to CAD layout of the proper dimensions. Table I presents expected frequencies for various beam dimensions, modes, and structural materials, showing a wide range of attainable frequencies, from VHF to UHF.

Although impressive at HF, the clamped-clamped beam device of Fig. 3 begins to lose a substantial fraction of its internal energy to the substrate at frequencies past 30 MHz, and this limits the attainable Q at VHF. To retain Q's around 8,000 at VHF, a beam with free-free ends is required, such as shown in Fig. 4, in which additional mechanical circuit complexity is added to allow free-free operation, and to reduce anchor losses to the substrate [9]. Via proper support beam design, anchor losses can be greatly attenuated in this structure, and Q's on the order of 8,000 are

Table I: μMechanical Resonator Frequency Design*

Freq. [MHz]	Material	Mode	h_r [μm]	W_r [μm]	L_r [μm]
70	silicon	1	2	8	14.54
110	silicon	1	2	8	11.26
250	silicon	1	2	4	6.74
870	silicon	2	2	4	4.38
1800	silicon	3	1	4	3.09
1800	diamond	3	1	4	6.16

* Determined for free-free beams using Timoshenko methods that include the effects of finite h and W_r [9].

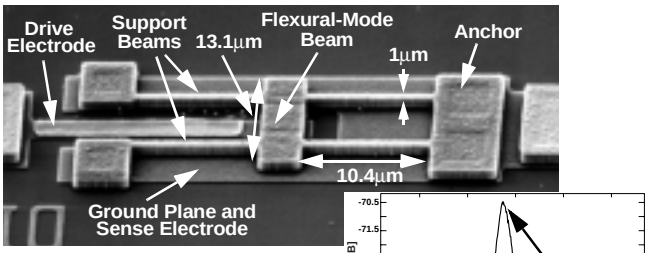

Fig. 4: SEM and measured frequency characteristic for a 92MHz free-free beam polysilicon μmechanical resonator [9].

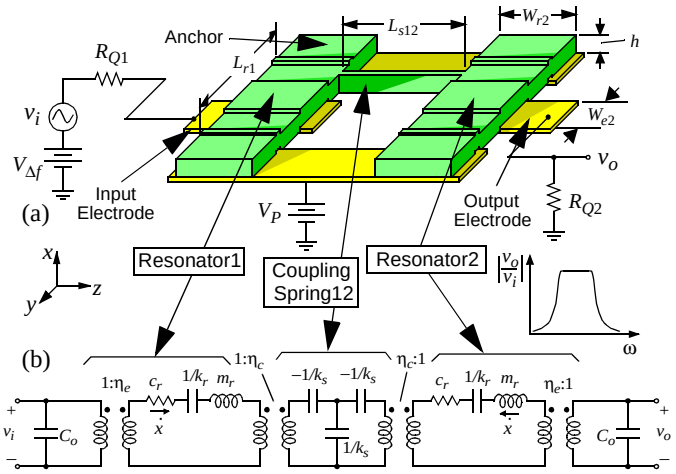

Fig. 5: (a) Schematic of a two-resonator micromechanical filter. (b) Equivalent circuit for the filter of (a) [8].

attained even at 92 MHz.

C. Micromechanical Filters

Among the more useful μmechanical circuits for communications are those implementing low-loss bandpass filters [8,11]. Figure 5(a) presents the perspective-view schematic of a two-resonator μmechanical filter, comprised of three mechanical links interconnected in a network designed to yield the bandpass spectrum shown in Fig. 5. The design of this filter has been covered extensively in previous literature [8]. For the present purposes, however, the operation of this filter can be deduced from its equivalent circuit, shown in Fig. 5(b). Here, each of the outside links serve as capacitively transduced μmechanical resonators, and so can be equated to *LCR* equivalent circuits. The connecting link actually operates as an acoustic transmission line, and thus, can be modeled by a *T*-network of energy storage elements. Finally, transformers model the electromechanical conversions at the I/O ports and the velocity transformations occurring at beam

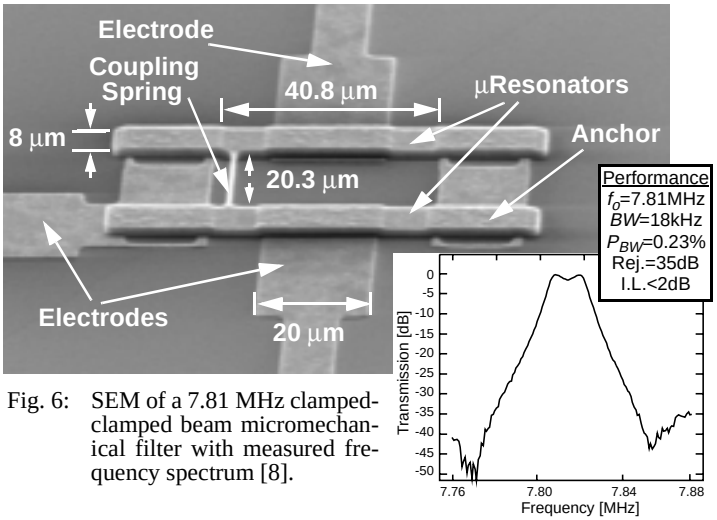

Fig. 6: SEM of a 7.81 MHz clamped-clamped beam micromechanical filter with measured frequency spectrum [8].

Table II: Two-Resonator μMechanical Filter Design*

	Gap Spacing, d				
R_Q [Ω]	300	500	1,000	2,000	5,000
f_o = 70 MHz	195Å	223Å	266Å	317Å	399Å
f_o = 870 MHz	78Å	81Å	80Å	95Å	119Å

* Determined with Q=10,000, BW=1.25MHz, V_P=10V.

connection points. Altogether, the complete circuit in Fig. 5(b) mimics that of an *LC* ladder bandpass filter, but with extremely high *Q*. The SEM for a fabricated 8.71 MHz filter with a measured spectrum is presented in Fig. 6.

As shown in Fig. 5(a), this filter is excited in a similar fashion to that described in the previous sub-section, with a dc-bias voltage V_P applied to the conductive mechanical network, and an ac signal applied to the input electrode, but this time through an appropriately valued source resistance that loads the *Q* of the input resonator to flatten the passband [8]. The output resonator of the filter must also see a matched impedance to avoid passband distortion. If the filter is designed symmetrically, with resonator *Q*'s much greater than that of the filter Q_{fltr}, the required value of I/O port termination resistance can be tailored for different applications via the expression

$$R_Q \cong \frac{\sqrt{k_{re} m_{re}}}{q Q_{fltr} \eta_e^2} = \frac{k_{re}}{\omega_o q Q_{fltr} \eta_e^2}. \qquad (4)$$

where *e* denotes the center location of the electrode, and *q* is a normalized constant obtainable from filter cookbooks [12]. Of the variables in (4), the electromechanical coupling factor η_e is often the most convenient to adjust for a desired value of termination resistance. Given that $\eta_e \sim (V_P/d^2)$, where *d* is the electrode-to-resonator gap spacing [8], termination impedance R_Q requirements and bias voltage V_P limitations often dictate the electrode-to-resonator gap spacing for a particular resonator design. This can be seen in Table II.

Note that Fig. 5 depicts a relatively simple mechanical circuit. Using more complicated interconnections with a larger number of beam elements and I/O ports, a wide variety of frequency-selective signal processing transfer functions can be realized, with even wider application ranges. From a circuit design perspective, the main difference between mechanical links and transistors are the basic features that make them useful as circuit elements: while transistors exhibit high gain, mechanical links exhibit very large *Q*. By combining the strong points of both circuit elements, on-chip functions previously unachievable are now within the realm of possibilities.

D. Micromechanical Mixer-Filters

As indicated by (1), the voltage-to-force transducer used by the described resonators is nonlinear, relating input force F_d to input voltage (v_e–v_b) by a square law. When v_b=V_P, this nonlinearity is suppressed, leading to a dominant force that is linear with v_e given by the second term of (2). If, however, signal inputs are applied to both v_e and v_b, a square law mixer results. In particular, if an RF signal v_{RF}=V_{RF}cos$\omega_{RF}t$ is applied to electrode *e*, and a local oscillator signal v_{LO}=V_{LO}cos$\omega_{LO}t$ to electrode *b*, then (1) contains the term

$$F_d = \ldots + \frac{1}{2} V_{RF} V_{LO} \frac{\partial C}{\partial x} \cos(\omega_{RF} - \omega_{LO})t + \ldots \qquad (5)$$

which clearly indicates a mixing of *voltage* signals v_{RF} and v_{LO} down to a *force* signal at frequency ω_{IF}=(ω_{RF}–ω_{LO}). If the above transducer is used to couple into a μmechanical filter with a pass-band centered at ω_{IF}, an effective mixer-filter device results that provides both a mixer and filtering function in one passive, μmechanical device.

Figure 7(a) presents the schematic for a symmetrical μmechanical mixer-filter [13], showing the bias and input scheme required for down-conversion and equating this device to a system-level functional block. As shown, since this device provides filtering as part of its function, the overall mechanical structure is exactly that of a μmechanical filter. The only differences are the applied inputs and the use of a non-conductive coupling beam to isolate the IF port from the LO. Note that if the source providing V_P to the second resonator is ideal (with zero source resistance) and the series resistance in the second resonator is small, LO signals feeding across the coupling beam capacitance are shunted to ac ground before reaching the IF port. In reality, finite resistivity in the resonator material allows some amount of LO-to-IF leakage.

The SSB noise figure NF_{mf} for this device derives from a combination of mixer conversion loss, filter insertion loss, and an additional 3dB that accounts for noise conversion from two bands (RF and image) to one. Although the first demonstrated mixer-filter based on polysilicon clamped-clamped beam μmechanical resonators achieved NF_{mf}=15dB [13], theory predicts that it is not unreasonable for such devices to eventually achieve NF_{mf} below 3.5 dB, given proper electrode design and using free-free beams for the resonators.

E. Micromechanical Switches

The mixer-filter device described above is one example of a μmechanical circuit that harnesses nonlinear device properties to provide a useful function. Another very useful mode of operation that further utilizes the nonlinear nature of the device is the μmechanical switch [14]. Figure 8 presents an operational schematic for a single-pole, single-throw μmechanical switch, seen to have a structure very similar to that of the previous resonator devices: a conductive beam or membrane suspended above an actuating electrode. The operation of the switch of Fig. 8 is fairly simple:

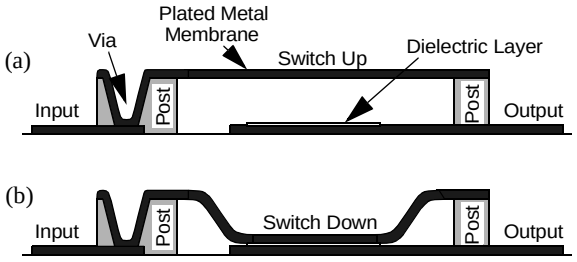

Fig. 8: Cross-sectional schematics of a typical μmechanical switch: (a) Switch up. (b) Switch down [14].

To achieve the "on-state", apply a sufficiently large voltage across the beam and electrode to generate a large force (given by the first term in (2)) that pulls the beam down and shorts it (in either a dc or ac fashion) to the electrode.

In general, to minimize insertion loss, the majority of switches use metals as their structural materials. It is their metal construction that makes μmechanical switches so attractive, allowing them to achieve "on-state" insertion losses down to 0.1 dB—much lower than FET transistor counterparts, which normally exhibit ~2 dB of insertion loss. In addition to exhibiting such low insertion loss, μmechanical switches are extremely linear, with *IIP3*'s greater than 66 dBm [1], and can be designed to consume no dc power (as opposed to FET switches, which sink a finite current when activated).

III. RF Receiver Front-End Architectures Using MEMS

Having surveyed a subset of the mechanical circuits most useful for communication applications, we now consider methods by which these circuits are best incorporated into communication receivers. Three approaches to using μmechanical vibrating resonators are described in order of increasing performance enhancement: (1) direct replacement of off-chip high-*Q* passives; (2) use of an RF channel select architecture using a large number of high-*Q* μmechanical resonators in filter banks and switchable networks; and (3) use of an all-mechanical RF front-end. Since the methods for achieving multi-band reconfigurability using MEMS are obvious, the majority of the discussion in this section will focus on power savings issues.

In proposing these architectures, certain liberties are taken in an attempt to account for potential advances in μmechanical resonator technology. For example, in the RF channel-select architecture, μmechanical circuits are assumed to be able to operate at UHF with *Q*'s on the order of 10,000. Given that thin-film bulk acoustic resonators (TFR's) [15]—arguably, MEMS devices in their own right—already operate at UHF (but with *Q*'s of 1,000), and 100MHz free-free beam μmechanical resonators presently exhibit *Q*'s around 8,000, the above assumed performance values may, in fact, not be far away. At any rate, the rather liberal approach taken in this section is largely beneficial, since it better conveys the potential future impact of MEMS technology, and

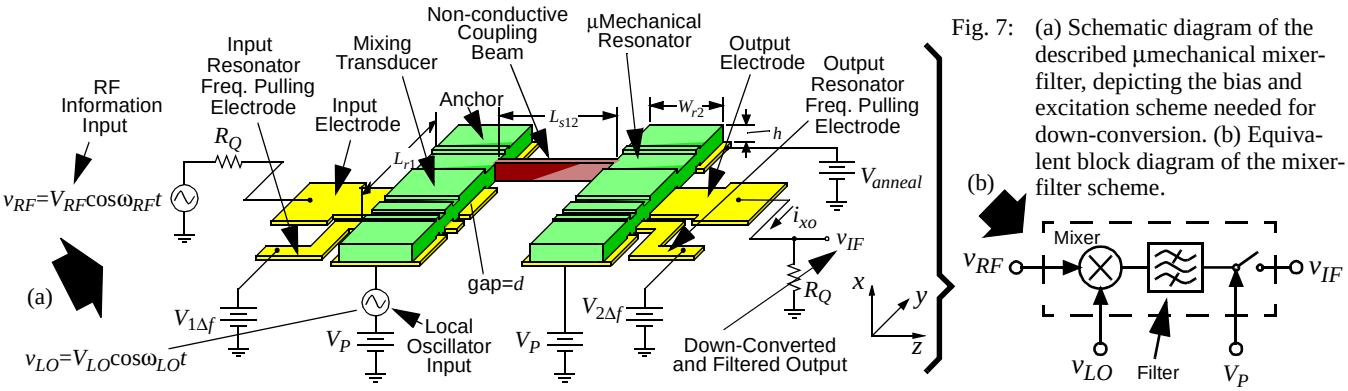

Fig. 7: (a) Schematic diagram of the described μmechanical mixer-filter, depicting the bias and excitation scheme needed for down-conversion. (b) Equivalent block diagram of the mixer-filter scheme.

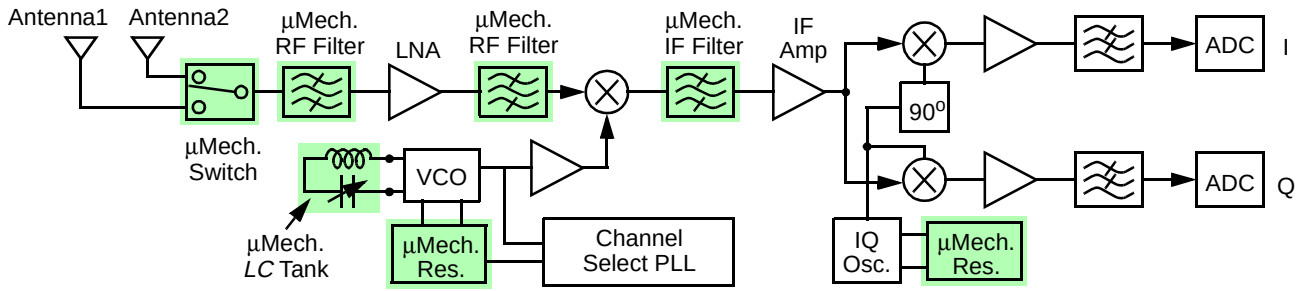

Fig. 9: System block diagram of a super-heterodyne receiver architecture showing potential replacements via MEMS-based components. (On-chip µmechanics are shaded.)

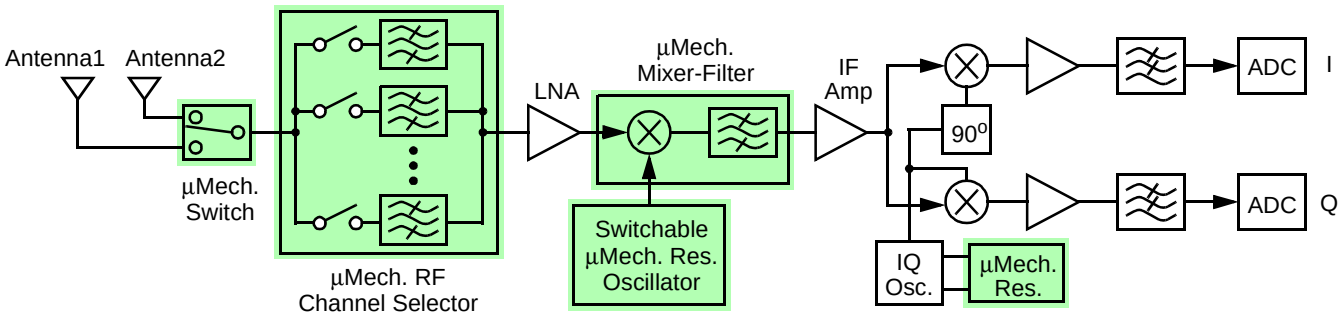

Fig. 10: System block diagram for an RF channel-select receiver architecture utilizing large numbers of micromechanical resonators in banks to trade Q for power consumption. (On-chip µmechanics are shaded.)

provides incentive for further advancements in this area. Nevertheless, in order to keep in check the enthusiasm generated here, assumed performances in this section are briefly re-evaluated in the next, with an eye towards practical implementation issues.

A. Direct Replacement of Off-Chip High-Q Passives

Perhaps the most direct way to harness µmechanical circuits is via direct replacement of the off-chip ceramic, SAW, and crystal resonators used in RF preselect and image reject filters, IF channel-select filters, and crystal oscillator references. A schematic depicting this approach is shown in Fig. 9. In addition to high-Q components, Fig. 9 also shows the use of other MEMS-based passive components, such as medium-Q micromachined inductors [1] and tunable capacitors [1] used in VCO's and matching networks, as well as low-loss (~0.1dB) µmechanical switches [14] that not only provide enhanced antenna diversity, but that can also yield enormous power savings by virtue of their extremely low loss, and by making TDD (rather than FDD) more practical in future transceivers.

Of course, the main benefits from the above approach to using MEMS are size reduction and, given the potential for integration of MEMS with transistor circuits, the ability to move more components onto the silicon die. A limited number of performance benefits also result from replacement of existing high-Q passives by µmechanical ones, such as the ability to tailor the termination impedances required by RF and IF filters (c.f., Table II). Such impedance flexibility can be beneficial when designing low-noise amplifiers (LNA's) and mixers in CMOS technology, which presently often consume additional power to impedance match their outputs to 50Ω off-chip components. If higher impedances can be used, for example at the output of an LNA, significant power savings are possible. As an additional benefit, since the source impedance presented to the LNA input is now equal to R_Q, it can now be tailored to minimize noise figure (*NF*).

Although beneficial, the performance gains afforded by mere direct replacement by MEMS are quite limited when compared to more aggressive uses of MEMS technology. More aggressive architectures will now be described.

B. An RF Channel-Select Architecture

To fully harness the advantages of µmechanical circuits, one must first recognize that due to their micro-scale size and zero dc power consumption, µmechanical circuits offer the same system complexity advantages over off-chip discrete components that planar IC circuits offer over discrete transistor circuits. Thus, to maximize performance gains, µmechanical circuits should be utilized on a massive scale. Figure 10 presents the system-level block diagram for a possible receiver front-end architecture that takes full advantage of the complexity achievable via µmechanical circuits. The main driving force behind this architecture is power reduction, attained in several of the blocks by trading power for high selectivity (i.e., high-Q). The key power saving blocks in Fig. 10 are now described.

Switchable RF Channel Select Filter Bank.

If channel selection (rather than pre-selection) were possible at RF frequencies (rather than just at IF), then succeeding electronic blocks in the receive path (e.g., LNA, mixer) would no longer need to handle the power of alternate channel interferers. Thus, their dynamic range can be greatly relaxed, allowing substantial power reductions. In addition, the rejection of adjacent channel interferers also allows reductions in the phase noise requirements of local oscillator (LO) synthesizers, providing further power savings.

To date, RF channel selection has been difficult to realize via present-day technologies. In particular, low-loss channel selection at RF would require tunable resonators with Q's in the thousands. Unfortunately, however, high-Q often precludes tunability, making RF channel selection via a single RF filter a very difficult prospect. On the other hand, it is still possible to select individual RF channels via many non-tunable high-Q filters, one for each channel, and each switchable by command. Depending upon the communication standard, this could entail hundreds or thousands of filters—numbers that would be absurd if off-chip macroscopic filters are used, but that may be perfectly reasonable for micro-scale, passive, µmechanical filters.

Figure 11 presents one fairly simple rendition of the key system block that realizes the desired RF channel selection. As shown, this block consists of a bank of µmechanical filters with all filter inputs connected to a common block input and all outputs to a common block output, and where each filter passband

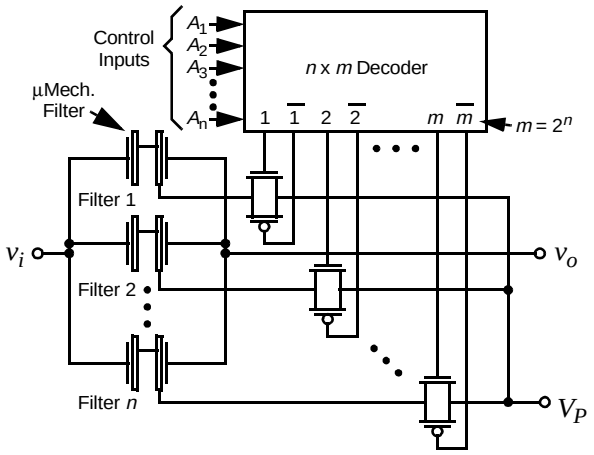

Fig. 11: System/circuit diagram for an RF channel-select micromechanical filter bank.

corresponds to a single channel in the standard of interest. In the scheme of Fig. 11, a given filter is switched on (with all others off) by decoder-controlled application of an appropriate dc-bias voltage to the desired filter. (Recall from (1) and (2) that the desired force input and output current are generated in a μmechanical resonator only when a dc-bias V_P is applied; i.e., without V_P, there's effectively an open across the I/O electrodes.)

The potential benefits afforded by this RF channel selector can be quantified by assessing its impact on the LNA linearity specification imposed by the IS-98-A interim standard for CDMA cellular mobile stations [16]. In this standard, the required IIP3 of the LNA is set mainly to avoid desensitization in the presence of a single tone (generated by AMPS [17]) spaced 900kHz away from the CDMA signal center frequency. Here, reciprocal mixing of the local oscillator phase noise with the 900kHz offset single tone and cross-modulation of the single tone with leaked transmitter power outputs dictate that the LNA IIP3 exceeds +7.6dBm [17]. However, if an RF channel select filter bank such as shown in Fig. 11 precedes the LNA and is able to reject the single tone by 40dB, the requirement on the LNA then relaxes to IIP3 ≤ −29.3dBm (assuming the phase noise specification of the local oscillator is *not* also relaxed). Given the well-known noise versus power trade-offs available in LNA design [18], such a relaxation in IIP3 can result in nearly an order of magnitude reduction in power. In addition, since RF channel selection relaxes the overall receiver linearity requirements, it may become possible to put more gain in the LNA to suppress noise figure (*NF*) contributions from later stages, while relaxing the required *NF* of the LNA itself, leading to further power savings.

Turning to oscillator power, if the single tone is attenuated to 40dB, then reciprocal mixing with the local oscillator is also greatly attenuated, allowing substantial reduction in the phase noise requirement of the local oscillator. Requirement reductions can easily be such that on-chip solutions to realization of the receive path VCO (e.g., using spiral inductors and pn-diode tunable capacitors [19]) become plausible.

Switchable Micromechanical Resonator Synthesizer.

Although the μmechanical RF channel-selector described above may make possible the use of existing on-chip technologies to realize the receive path VCO, this approach is not recommended, since it denies the system from achieving much greater power reduction factors that may soon be available through MEMS technology. In particular, given that power and *Q* can often be interchanged when designing for a given oscillator phase noise specification, a better approach to implementing the VCO would be to use μmechanical resonators (with orders of magnitude higher *Q* than any other on-chip tank) to set the VCO frequency. In fact, with *Q*'s as high as achievable via μmechanics, the basic design methodologies for oscillators must be re-evaluated. For example, in the case where the oscillator and its output buffer contribute phase noise according to Leeson's equation [20], where the $1/f^2$-to-white phase noise corner occurs at $(f_o/(2Q))$, a tank Q>1,500 is all that would be required to move the $1/f^2$-to-white phase noise corner close enough to the carrier that only white phase noise need be considered for CDMA cellular applications, where the phase noise power at frequency offsets from 285kHz to 1515kHz is most important. If only white noise is important, then only the output buffer noise need be minimized, and sustaining amplifier noise may not even be an issue. If so, the power requirement in the sustaining amplifier might be dictated solely by loop gain needs (rather than by phase noise needs), which for a μmechanical resonator-based VCO with R_x~40Ω, L_x~84μH, and C_x~0.5fF, might be less than 1mW.

To implement a tunable local oscillator synthesizer, a switchable bank is needed, similar to that of Fig. 11 but using μmechanical resonators, not filters, each corresponding to one of the needed LO frequencies, and each switchable into or out of the oscillator sustaining circuit. Note that because μmechanical resonators are now used in this implementation, the *Q* and thermal stability (with compensation electronics) of the oscillator may now be sufficient to operate without the need for locking to a lower frequency crystal reference. The power savings attained upon removing the PLL and prescaler electronics needed in past synthesizers can obviously be quite substantial. In effect, by implementing the synthesizer using μmechanical resonators, synthesizer power consumption can be reduced from the ~90mW dissipated by present-day implementations using medium-*Q L* and *C* components [21], to something in the range of only 1-4 mW. Again, all this is attained using a circuit topology that would seem absurd if only macroscopic high-*Q* resonators were available, but that becomes plausible in the micromechanical arena.

Micromechanical Mixer-Filter.

The use of a μmechanical mixer-filter in the receive path of Fig. 10 eliminates the dc power consumption associated with the active mixer normally used in present-day receiver architectures. This corresponds to a power savings on the order of 10-20 mW. In addition, if multiple input electrodes (one for RF, one for matching) are used for the mixer-filter, its RF input impedance can be tailored to simplify the design of the driver stage in the LNA, allowing power savings similar to that discussed in Section III.A.

C. An All-MEMS RF Front-End Receiver Architecture

In discussing the above MEMS-based architecture, one very valid question may have arisen: If μmechanical filters and mixer-filters can truly post insertion losses consistent with their high-*Q* characteristics, then is an LNA really required at RF frequencies? It is this question that inspires the receiver architecture shown in Fig. 12, which depicts a receive path comprised of a relatively wideband image reject μmechanical RF filter followed immediately by a narrowband IF mixer-filter that then feeds subsequent IF electronics. The only active electronics operating at RF in this system are those associated with the local oscillator, which if it uses a bank of μmechanical resonators as described in the previous section, can operate at 1-4 mW. If plausible, the architecture of Fig. 12 clearly presents enormous power advantages, eliminating completely the 40-50 mW combined power consumption of the LNA and active mixer of Fig. 9, and together with LO power savings, substantially increasing mobile phone standby times.

To assess the plausibility of this all-MEMS front-end, one can determine whether or not this scheme yields a reasonable noise figure requirement at the input node of the IF amplifier in Fig. 12. An expected value for RF image reject filter insertion loss is *IL*~0.2dB, assuming that three resonators are used, each with

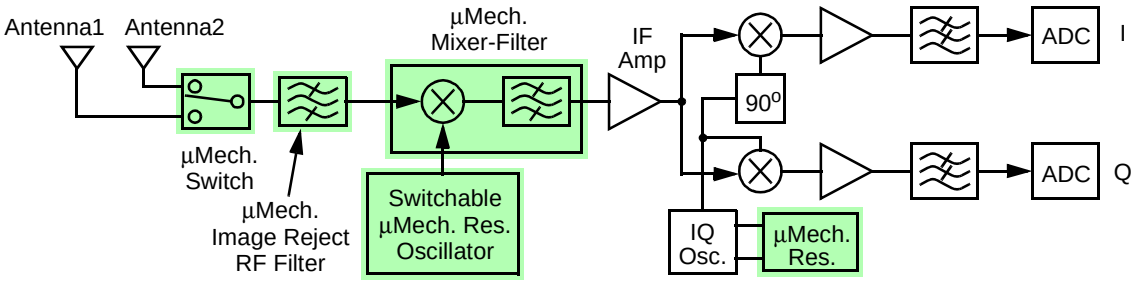

Fig. 12: System-block diagram for an all-MEMS RF front-end receiver architecture. (On-chip μmechanics are shaded.)

Q=5,000. Using the value for mixer-filter NF_{mf}=3.5dB projected in Section II, the total combined NF_{f+mf}=3.7dB. Given IS-98-A's requirement that the receiver NF_{RX}≤7.8dB, the needed value at the IF amplifier input is NF_{IF}≤4.1dB, which can be reasonable if the IF amplifier gain can be increased to suppress the noise of succeeding stages.

Although the all-MEMS front-end architecture of Fig. 12 may at first seem the most preposterous of the bunch, early versions of the primary filtering and mixing devices required for its implementation have already been demonstrated. In particular, TFR image-reject filters have been demonstrated at UHF frequencies with insertion losses of less than 3dB [15]. In addition, although not yet demonstrated with the needed noise figure, mixer-filter devices have already been demonstrated with the required RF and IF frequency ranges [13], as mentioned in Section II. With improvements in mixer-filter noise figure and eventual realization of projected frequency increases for μmechanical filters, the receiver topology of Fig. 12 may soon become reasonable.

IV. Research Issues

As stated at the beginning of Section III, the receiver architectures described above rely to some extent on performance characteristics not yet attained by μmechanical resonators, but targeted by ongoing research efforts. Specifically, μmechanical devices with the following attributes have been assumed: (1) adequate Q at UHF frequencies; (2) sufficient linearity and power handling capability; (3) usable port impedances; and (4) massive scale integration methods.

A. Frequency and Q

Table I of Section II showed that from a purely geometric perspective, the frequencies required by the architectures of Section III are reasonable. However, frequency is not really the main issue; Q is. The most important question is whether high-Q can be maintained as frequencies increase, since new loss mechanisms may be introduced as frequencies increase. Section II.B presented one example of this, where anchor losses in clamped-clamped beams become excessive past 50MHz, making free-free beams (that effectively remove anchors) much more suitable for mid-VHF and UHF frequencies [9]. What loss mechanisms await at GHz frequencies for flexural-mode resonators is, as yet, unknown. However, as mentioned previously, Q's of over 1,000 at UHF (and beyond) have already been achieved via thin-film bulk acoustic resonators based on longitudinal resonance modes and piezoelectric structural materials. It is hoped that μmechanical resonators can retain Q's of at least 8,000 at similar frequencies [22], which would make plausible the RF channel-selector of Fig. 11.

B. Linearity and Power Handling

Macroscopic high-Q filters based on ceramic resonator or SAW technologies are very linear in comparison with the transistor blocks they interface with in present-day transceivers. As a result, their contributions the total IIP3 budget can generally be ignored in the majority of designs. Although capacitively transduced μmechanical resonators are generally more linear than transistor circuits, with semi-empirical IIP3's of +12dB for 2μm-thick 70MHz resonators [8], they are still less linear than some of their off-chip macroscopic counterparts. The degree to which this impacts the utility of the architectures proposed in Section III depends upon the standard being implemented. For example, an IIP3 of +12dB is sufficient for most receive applications, except for those in standards that allow simultaneous transmit and receive (such as CDMA), where the RF preselect filter is required to reject out-of-band transmitter outputs to alleviate cross-modulation phenomena [17]. For such situations, at least at present, a more linear filter must precede the filter bank of Fig. 11 if cross-modulation is to be sufficiently suppressed. This additional filter, however, can now have a very wide bandwidth, as it has no other purpose than to reject transmitter outputs. Thus, it may be realizable with very little insertion loss using on-chip (perhaps micromachined) inductor and capacitor technologies [1].

Still, μmechanical circuits with high power handling capability would not only present a better solution to the above, but if usable with transmit powers, might also enable substantial power savings in the transmit path by allowing relaxed linearity in the power amplifier. Pursuant to higher power handling ability, alternative geometries (e.g., no longer flexural mode) and the use of alternative transduction methods (e.g., piezoelectric, magnetostrictive) are presently under study. Techniques for combining devices to increase power capacity are also being explored.

C. Resonator Impedance

Thin-film bulk acoustic resonators can already impedance match to conventional antennas, so if their frequency, Q, yield, size, and integration capacity are adequate for a given architecture (e.g., the all-MEMS architecture of Section III), then they present a very good solution. If higher Q is needed, however, then μmechanical resonators may be better suited for the given application. From Table II, RF μmechanical filters should be able to match to 300Ω impedances, provided their electrode-to-resonator gaps can be made down to d~80Å. Since electrode-to-resonator gaps are achieved via a process very similar to that used to achieve MOS gate oxides [8], such gaps are not unreasonable. However, device linearity generally degrades with decreasing d, so practical designs must balance linearity with impedance requirements [8].

D. Fabrication Technologies

To date, surface micromachining technologies have been used quite successfully to realize fully integrated circuit-MEMS products in high volume, and in some cases, at VLSI complexities [2,3]. In addition, adaptive circuit-MEMS technologies are now emerging that separate the circuits and MEMS processes into modules, allowing integration of virtually any circuit process with a given MEMS technology. A variety of modular integration approaches have recently been demonstrated, including fully planar processes where the MEMS module is done either before [4] or after [5] the circuits module (c.f., Fig. 13), as well as techniques based upon wafer-level bonding [24] (perhaps the ultimate in modularity). Meanwhile, on-chip vacuum encapsulation processes (needed for high-Q and environmental protection) are also

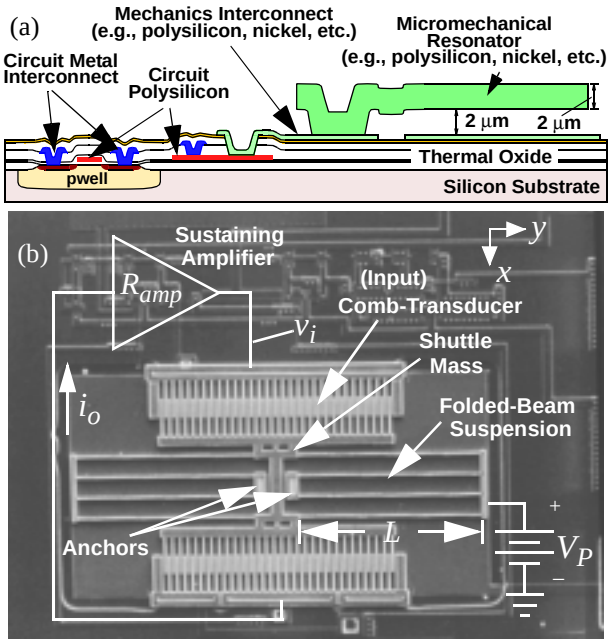

Fig. 13: (a) Cross-section of the MICS process, which modularly merges CMOS transistors with surface-micromachined μmechanics (circuits before mechanics) [23]. (b) Overhead-view of a fully integrated μmechanical resonator oscillator fabricated using MICS [23].

receiving focused attention, with many approaches now under study, including ones based upon bonding technologies [24], and others based upon planar processing where three or four additional masking steps are utilized to form sealable caps over microstructures [25]. Finally, frequency trimming methods are also a subject of ongoing research [26].

From a cost perspective, which technology is best depends to a large extent on how much of the chip area is consumed by MEMS devices in the application in question. For cases where the MEMS utilizes only a small percentage of the chip area, bonding approaches may be more economical, since a larger number of MEMS chips can be achieved on a dedicated wafer. For cases where MEMS devices take up a large amount of chip area, or where node capacitance must be minimized for highest performance, planar integration may make more sense.

V. Conclusions

Vibrating μmechanical resonators constitute the building blocks for a new integrated mechanical circuit technology in which high *Q* serves as a principal design parameter that enables more complex circuits. By combining the strengths of integrated μmechanical and transistor circuits, using both in massive quantities, previously unachievable functions become possible that enable transceiver architectures with projections for orders of magnitude performance gains. In particular, with the addition of high-*Q* μmechanical circuits, paradigm-shifting transceiver architectures that trade power for selectivity (i.e., *Q*) become possible, with the potential for substantial power savings and multi-band reconfigurability. To reap the benefits of these new architectures, however, further advancements in device frequency, linearity, and manufacturability are required. Research efforts are ongoing.

References

[1] C. T.-C. Nguyen, L. P.B. Katehi, and G. M. Rebeiz, "Micromachined devices for wireless communications (invited)," *Proc. IEEE*, vol. 86, no. 8, pp. 1756-1768, Aug. 1998.

[2] T. A. Core, W. K. Tsang, S. J. Sherman, "Fabrication technology for an integrated surface-micromachined sensor," *Solid State Technology*, pp. 39-47, Oct. 1993.

[3] L. J. Hornbeck, T. R. Howell, R. L. Knipe, and M. A. Mignardi, "Digital micromirror device—commercialization of a massively parallel MEMS technology," *Microelectronic Systems 1997*, DSC-Vol. 62, ASME International Mechanical Engineering Congress and Exposition (1997), pp. 3-8.

[4] A. E. Franke, D. Bilic, D. T. Chang, P. T. Jones, T.-J. King, R. T. Howe, and G. C. Johnson, "Post-CMOS integration of germanium microstructures," *Technical Digest*, 12th Int. IEEE MEMS Conf., Orlando, Florida, Jan. 17-21, 1999, pp. 630-637.

[5] J. H. Smith, S. Montague, J. J. Sniegowski, J. R. Murray, *et al*., "Embedded micromechanical devices for the monolithic integration of MEMS with CMOS," *Proceedings*, IEEE Int.Electron Devices Meeting, Washington, D.C., Dec. 10-13, 1995, pp. 609-612.

[6] C. T.-C. Nguyen, "Frequency-selective MEMS for miniaturized low-power communication devices (invited)," *IEEE Trans. Microwave Theory Tech.*, vol. 47, no. 8, pp. 1486-1503, Aug. 1999.

[7] J. M. Bustillo, R. T. Howe, and R. S. Muller, "Surface micromachining for microelectromechanical systems," *Proc. IEEE*, vol. 86, no. 8, pp. 1552-1574, Aug. 1998.

[8] F. D. Bannon III, J. R. Clark, and C. T.-C. Nguyen, "High frequency micromechanical filters," *IEEE J. Solid-State Circuits*, vol. 35, no. 4, pp. 512-526, April 2000.

[9] K. Wang, Y. Yu, A.-C. Wong, and C. T.-C. Nguyen, "VHF free-free beam high-*Q* micromechanical resonators," *Technical Digest*, IEEE MEMS Conf., Orlando, Florida, Jan. 17-21, 1999, pp. 453-458.

[10] H. A. C. Tilmans and R. Legtenberg, "Electrostatically driven vacuum-encapsulated polysilicon resonators: Part II. Theory and performance," *Sensors and Actuators*, vol. A45 (1994), pp. 67-84.

[11] K. Wang and C. T.-C. Nguyen, "High-order medium frequency micromechanical electronic filters," *IEEE J. Microelectromech. Syst.*, vol. 8, no. 4, pp. 534-557, Dec. 1999.

[12] A. I. Zverev, *Handbook of Filter Synthesis*, New York: John Wiley & Sons, 1967.

[13] A.-C. Wong, H. Ding, and C. T.-C. Nguyen, "Micromechanical mixer+filters," *Technical Digest*, IEEE Int. Electron Devices Meeting, San Francisco, California, Dec. 6-9, 1998, pp. 471-474.

[14] Z. Jamie Yao, S. Chen, S. Eshelman, D. Denniston, and C. Goldsmith, "Micromachined low-loss microwave switches," *J. Microelectromech. Syst.*, vol. 8, no. 2, pp. 129-134, June 1999.

[15] K. M. Lakin, G. R. Kline, and K. T. McCarron, "Development of miniature filters for wireless applications," *IEEE Trans. Microwave Theory Tech.*, vol. 43, no. 12, pp. 2933-2939, Dec. 1995.

[16] "Recommended minimum performance standards for dual-mode wideband spread spectrum cellular mobile stations," *TIA/EIA/IS-98-A Interim Standard*, July 1996.

[17] W. Y. Ali-Ahmad, "RF system issues related to CDMA receiver specifications," *RF Design*, pp. 22-32, Sept. 1999.

[18] D. K. Shaeffer and T. H. Lee, "A 1.5-V, 1.5-GHz CMOS low noise amplifier," *IEEE J. Solid-State Circuits*, vol. 32, No. 5, pp. 745-759, May 1997.

[19] J. Craninckx and M. S. J. Steyaert, "A 1.8-GHz low-phase noise CMOS VCO using optimized hollow spiral inductors," *IEEE J. Solid-State Circuits*, vol. 32, no. 5, pp. 736-744, May 1997.

[20] D. B. Leeson, "A simple model of feedback oscillator noise spectrum," *Proc. IEEE*, vol. 54, pp. 329-330, Feb. 1966.

[21] J. F. Parker and D. Ray, "A 1.6-GHz CMOS PLL with on-chip loop filter," *IEEE J. Solid-State Circuits*, vol. 33, no. 3, pp. 337-343, March 1998.

[22] M. L. Roukes, "Nanoelectromechanical systems," *Tech. Digest*, 2000 Solid-State Sensor and Actuator Workshop, Hilton Head Island, South Carolina, June 4-8, 2000, pp. 367-376.

[23] C. T.-C. Nguyen and R. T. Howe, "An integrated CMOS micromechanical resonator high-*Q* oscillator," *IEEE J. Solid-State Circuits*, vol. 34, no. 4, pp. 440-445, April 1999.

[24] A. Singh, D. A. Horsley, M. B. Cohn, A. P. Pisano, and R. T. Howe, "Batch transfer of microstructures using flip-chip solder bonding," *J. Microelectromech. Syst.*, vol. 8, no. 1, pp. 27-33, March 1999.

[25] K. S. Lebouitz, A. Mazaheri, R. T. Howe, and A. P. Pisano, "Vacuum encapsulation of resonant devices using permeable polysilicon," *Technical Digest*, 12th International IEEE MEMS Conference, Orlando, Florida, Jan. 17-21, 1999, pp. 470-475.

[26] K. Wang, A.-C. Wong, W.-T. Hsu, and C. T.-C. Nguyen, "Frequency-trimming and *Q*-factor enhancement of micromechanical resonators via localized filament annealing," *Digest of Technical Papers*, Transducers'97, Chicago, Illinois, June 16-19, 1997, pp. 109-112.